Voltage Control of a Three-Phase Distribution Grid using a DC Microgrid-Fed STATCOM

Faeka M. Khater
Power Electronics and Energy Conversion Department, Electronic Research Institute, Egypt
khater@eri.sci.eg

Zeinab Elkady
Power Electronics and Energy Conversion Department, Electronic Research Institute, Egypt
zainab.elkady@eri.sci.eg

Amany M. Amr
Power Electronics and Energy Conversion Department, Electronic Research Institute, Egypt
amany_amr2016@f-eng.tanta.edu.eg (corresponding author)

Diaa-Eldin A. Mansour
Department of Electrical Power Engineering, Faculty of Engineering, Egypt-Japan University of Science and Technology (E-JUST), Egypt | Department of Electrical Power and Machines Engineering, Faculty of Engineering, Tanta University, Egypt
mansour@f-eng.tanta.edu.eg

Ahmed E. El Gebaly
Department of Electrical Power and Machines Engineering, Faculty of Engineering, Tanta University, Egypt
ahmed.elgebaly@f-eng.tanta.edu.eg

Received: 3 November 2023 | Revised: 7 December 2023 | Accepted: 8 December 2023

 DOI: https://doi.org/10.48084/etasr.6590

ABSTRACT

With the increasing penetration of microgrids in distribution systems, the possibility for voltage variations increases. This paper proposes the use of a static synchronous compensator (STATCOM) fed by a DC microgrid to control the voltage of a 3-phase AC distribution grid and provide bidirectional active power transfer from the AC grid to the DC microgrid and vice versa. A simplified control is applied to this system to manage the magnitude and angle of the system voltage at the point of common coupling. With the use of a PI controller and pulse width modulation, the proposed control was able to modify the active and reactive power compensation. The control approach is characterized by its simplicity and rapid response to system changes, such as fault occurrences or load variations. The proposed control system is applied after converting the 3-phase system into a dq system to simplify the voltage regulation process. The PSCAD package is used to perform the simulation. Results demonstrate that it is possible to control STATCOM to offset reactive power and regulate grid voltage. The results validated the ability of active power transfer through the line by injecting negative and positive active power. The transfer of active and reactive power from the AC grid to the DC microgrid, and vice versa, is examined in this study following the STATCOM rating and the energy management demands.

Keywords-static synchronous compensator (STATCOM); PI controller; FACTS; DC microgrid

I. INTRODUCTION

Renewable energy is playing an important role in shaping the future of energy as a clean and sustainable source [1, 2]. Recently, the development of renewable energy generation has seen significant progress. The prevailing energy trend is shifting towards renewable sources due to the advantages they offer, such as economic viability in various applications, ensured availability and sustainability, and environmental safety. Notable examples of renewable energy sources include photovoltaic (PV), wind, hydropower, tidal power, geothermal power, biomass power, and other systems [3].

In order to ensure the security of the energy supply, microgrids have emerged as a viable solution. A microgrid refers to a small-scale network that can independently supply power to loads, with or without assistance from the main grid [4]. A typical microgrid comprises batteries, loads, and interconnected renewable energy sources, all connected to the same bus. There are three main types of microgrids: DC, AC, and hybrid. Among these, the DC microgrid offers several advantages, including enhanced system stability, compact size, absence of synchronization, and reduced costs while using DC-based renewables and energy storage systems [5-7]. The AC distribution grid faces various power quality issues, such as voltage disturbances, harmonic distortion, unbalance among phases and low power factor. These problems not only disturb the normal operation of the system but also impact the performance of connected loads. Consequently, extensive studies have been carried out to address these issues and enhance the power quality of the grid through the utilization of power electronics-based devices, such as the Flexible AC Transmission Systems (FACTS). The major types of FACTS devices are the static synchronous compensator (STATCOM) and the Static VAR Compensator (SVC). The response time of STATCOM is faster than SVC [8, 9]. In order to keep the grid voltage at the Point of Common Coupling (PCC) within a particular range, reactive power is compensated with STATCOM [10].

STATCOM is considered a very important device widely used in power systems for various applications. For compensating reactive power, the STATCOM is proposed in [11] using a model of half bridge and modular multilevel converter. In [12], D-STATCOM is proposed to be used to mitigate unbalanced voltage characteristics resulting from the connection of a three-phase transformer bank in a distribution system. In [13], three various strategies were proposed to control STATCOM by controlling the voltage and reactive power. In [14], a STATCOM is designed to improve the low-voltage ride-through capability of grid-connected induction machines following grid faults by controlling the reference voltage, thereby limiting the maximum torque of the induction motor. A comparison between SVC and STATCOM was carried out in [15], while the applications of STATCOM for power quality improvement of grid-connected wind farms were described in [16, 17]. In [18], a PID controller with an adaptive switched filter capacitor and a modified D-STATCOM were proposed. The PID controller gains were optimally tuned using the grasshopper's optimization algorithm. A new mechanism is added in [19] as a secondary control to regulate the voltage of the DC-link. This mechanism is based on the magnitude of the modulation index and aims to keep the current total harmonic distortion within the standard range.

This paper proposes a new system aiming to provide voltage support for 3-phase AC grids through incorporating a STATCOM fed by a DC microgrid. The utilization of STATCOM facilitates the integration of the microgrid and the main grid and allows for precise control of the grid voltage. Also, the STATCOM regulates the active and reactive power flow between the main power grid and the microgrid. The main contributions of this article can be summarized as follows:

- A new structure for voltage support in 3-phase distribution grids using a DC microgrid interfaced via STATCOM is introduced.
- A decoupling control method for active and reactive power exchange between the grid and the microgrid is developed, in contradiction to previous studies which focused only on reactive power control.
- The proposed structure and control are validated in a real-time platform.

II. SYSTEM DESCRIPTION

The system consists of the AC grid, the STATCOM and a DC microgrid. Figure 1 illustrates the connection between the grid and the microgrid through STATCOM. A 3-phase star-earthed transformer is utilized to establish the connection between STATCOM and the AC grid. A 3-phase load is applied to the AC grid, with the load becoming operational after 5 s. An inductance is added between the PCC and the output of the transformer. In general, STATCOM consists of an inverter and a capacitor located in the DC link. The inverter consists of 6 Insulated-Gate Bipolar Transistors (IGBTs) designed to turn on and off rapidly. In this work, the microgrid is located on the DC link instead of the conventional capacitor. The microgrid, as depicted in Figure 2 [20], encompasses a PV system, a wind turbine system, two batteries, and loads. The 3-phase transformer is installed to connect between the two various voltage levels of the AC grid and the inverter's AC side.

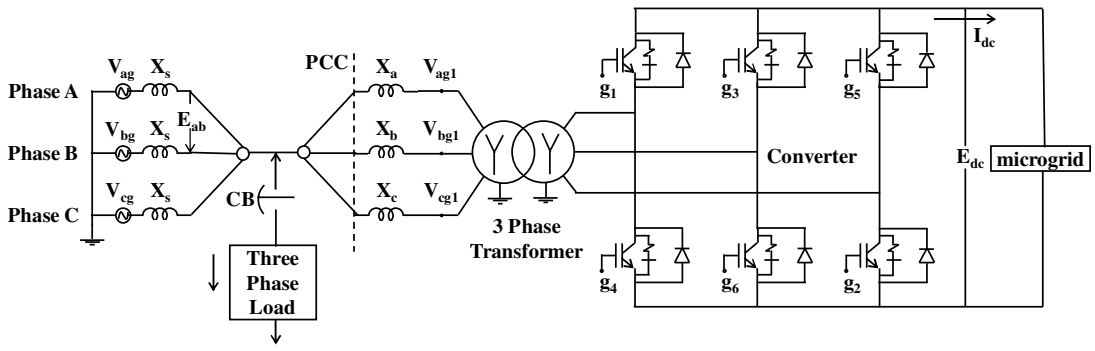

Fig. 1. Schematic diagram of the proposed system.

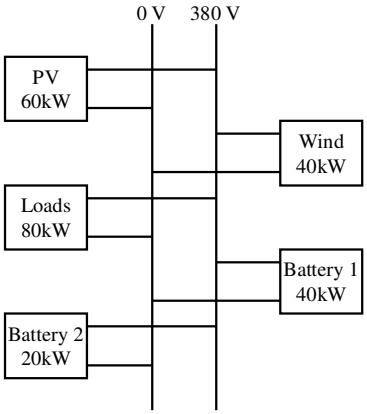

Fig. 2. Schematic diagram of the studied microgrid.

III. PRINCIPLE OF OPERATION OF STATCOM

In the family of FACTS electronic components, STATCOM is a key component that is shunt connected with the system. A power network's stability is boosted by STATCOM's capacity to control the flow of reactive power through the system. The term "synchronous" in STATCOM refers to the ability to generate or absorb reactive power in time with the need to maintain the power network's voltage. The 3-phase AC power grid system was studied in this work. The type of power electronic switches of the inverter is IGBT. The advantages of IGBT over others are that the IGBT has high power density, small size, high reliability, and low cost [21].

Figure 3 shows the characteristic curve of an STATCOM. STATCOM is regarded as an inductive or capacitive current source. According to the power system parameters and the slope of the STATCOM parameters, the injected current can modify the voltage of the PCC. The maximum capacitive or inductive current limits can be determined using STATCOM component ratings. Due to the brief duration of transient events, the transient ratings are slightly higher than the nominal ratings. An example of how the STATCOM can adjust the PCC voltage by reactive power compensation is illustrated in Figure 4. Reactive power compensation needs a certain value of capacitor current to adjust the grid voltage at the reference value. If the value of system voltage V_s is reduced to 0.7 pu, the line characteristics of the system intersect with the characteristics of STATCOM at point X which refers to X_1, corresponding to capacitor current I_x. The value of X_1 (about 0.95 pu) closes to the reference voltage of 1 pu. This improvement of voltage is due to the capacitor current I_x and reactive power compensator [22, 23]. Figure 5 shows the schematic diagram of the STATCOM device, where the STATCOM is represented by the inverter and the capacitor. It is connected to the power grid through an impedance consisting of both resistance and inductance [23]. The equivalent circuit of the STATCOM, as depicted in Figure 6, comprises two voltage sources. The AC voltage source represents the grid, while the controlled voltage source E_{dc} represents the STATCOM. The impedance between these two voltage sources includes both resistance and inductance. Assuming negligible internal losses in the link between the voltage sources V_s and E_{dc}, the resistance R can be considered as being equal to 0. The active and reactive power flowing through the line are determined by:

$$P = \frac{V_S E_{dc} \sin \delta}{X} \quad (1)$$

$$Q = \frac{E_{dc} (V_S \cos \delta - E_{dc})}{X} \quad (2)$$

where V_S is the AC voltage source of the grid, E_{dc} is the DC voltage source on the capacitor, and δ is the load angle between V_s and E_{dc}.

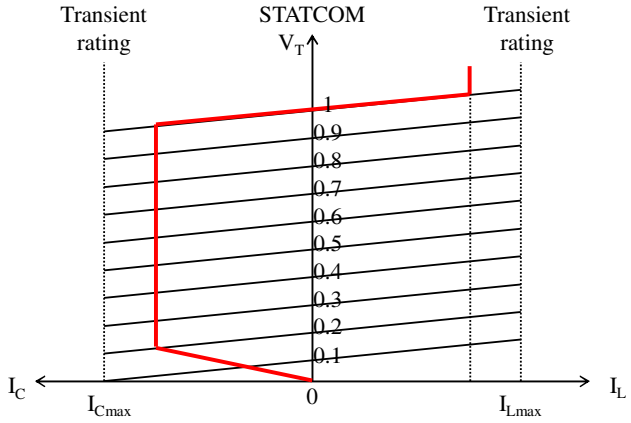

Fig. 3. Characteristic curve of the STATCOM.

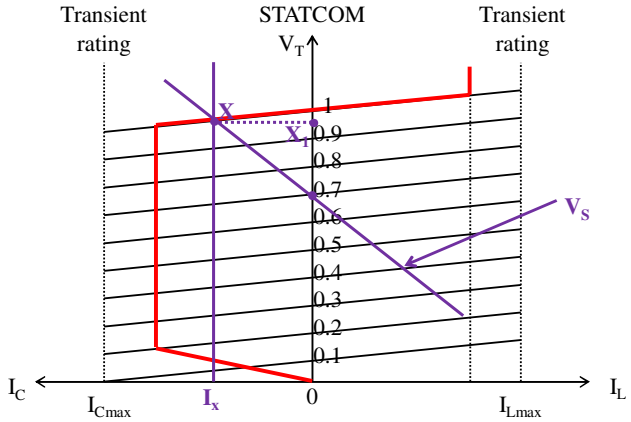

Fig. 4. Example of STATCOM operation and adjustment.

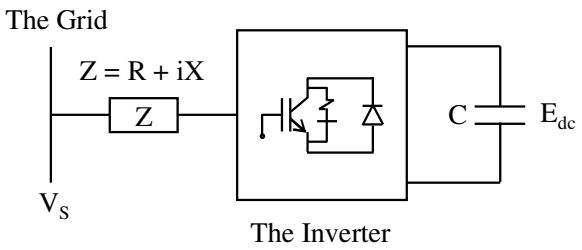

Fig. 5. Schematic diagram of the STATCOM device.

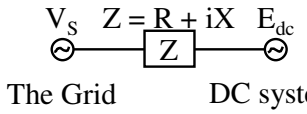

Fig. 6. Equivalent circuit of the STATCOM device.

When the load angle δ equals to 0, the transferred active power P and reactive power Q can be determined by:

$$P = 0 \quad (3)$$

$$Q = \frac{E_{dc}\,(V_S - E_{dc})}{X} \quad (4)$$

The previous equations explain the relation between the reactive power and the magnitude of the voltage and the relation between the active power and the angle. STATCOM operates on this guiding idea [24]. The formulation of a specific magnitude of voltage E_{dc} determines how STATCOM controls the reactive power flow via the line. Also, active power can be transferred through the system.

IV. VOLTAGE CONTROL OF STATCOM CONNECTED TO THE MICROGRID AT THE DC SIDE

The goal in this study is to maintain a constant value for the 3-phase voltage of the AC system at the PCC. Another goal is to regulate the active power flow between the grid and the DC system based on energy management requirements. The control method proposed in this study is presented in Figure 7, which consists of three steps. In the first step, the 3-phase voltage of the grid is converted into a simplified 2-phase system. This conversion is performed to facilitate the control process. The second step involves applying the control method to the newly obtained 2-phase system. Finally, in the third step, the 2-phase system is transformed back into a 3-phase system to enable the application of Pulse Width Modulation (PWM).

In Figure 7, the grid voltage (V_{ag}, V_{bg}, and V_{cg}) is converted into a dq0 rotating reference frame (V_d, V_q, and V_0). This transformation to the dq0 frame is crucial because it simplifies the control process by decoupling the control of two axes. V_q is responsible for adjusting the reactive power and consequently the voltage, while V_d is responsible for regulating the active power and hence the phase difference (δ). The equations of converting abc axes to dq0 axes are:

$$V_d = \frac{2}{3}\left(V_{ag}\sin(\omega t) + V_{bg}\sin\left(\omega t - \frac{2\pi}{3}\right) + V_{cg}\sin\left(\omega t + \frac{2\pi}{3}\right)\right) \quad (5)$$

$$V_q = \frac{2}{3}\left(V_{ag}\cos(\omega t) + V_{bg}\cos\left(\omega t - \frac{2\pi}{3}\right) + V_{cg}\cos\left(\omega t + \frac{2\pi}{3}\right)\right) \quad (6)$$

$$V_0 = \frac{1}{3}\left(V_{ag} + V_{bg} + V_{cg}\right) \quad (7)$$

where V_d, V_q, and V_0 represent the output voltage from converting abc to dq0 and V_{ag}, V_{bg}, and V_{cg} represent the voltage of the grid system at the PCC of phases A, B and C.

The PI controller is used to control V_d and V_q. The PI controller coefficients are: integral time constant of 0.005 s and proportional gain of 10. The output signals of the controller V_{d1} and V_{q1} are converted from dq0 (V_{d1} and V_{q1}) to abc (V_{aa}, V_{ab} and V_{ac}). The conversion from dq0 axes to abc axes is shown in (8)-(10). The signals V_{aa}, V_{ab} and V_{ac} are the inputs to PWM used to control the six IGBT signals as given in Figure 8. The input signals to the PWM device are the 3-phase outputs from the dqo/abc device. The PWM device compares these 3-phase signals and triangle functions to obtain the control signals for the gates of the IGBT devices that are responsible for controlling the grid voltage. Control and PWM are simulated in the PSCAD package. For controlling the voltage, V_{qref} will be adjusted to the reference value that controls the reactive power transfer in the system and therefore the voltage of the system. V_{dref} will be adjusted to the reference value that controls the active power transfer in the system and therefore the angle of the system.

$$V_{aa} = V_{d1}\sin(\omega t) + V_{q1}\cos(\omega t) + V_0 \quad (8)$$

$$V_{ab} = V_{d1}\sin\left(\omega t - \frac{2\pi}{3}\right) + V_{q1}\cos\left(\omega t - \frac{2\pi}{3}\right) + V_0 \quad (9)$$

$$V_{ac} = V_{d1}\sin\left(\omega t + \frac{2\pi}{3}\right) + V_{q1}\cos\left(\omega t + \frac{2\pi}{3}\right) + V_0 \quad (10)$$

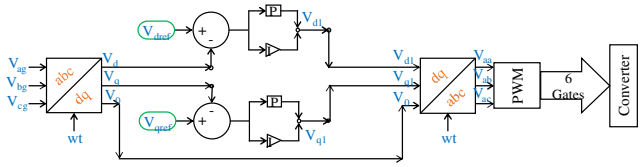

Fig. 7. Proposed control structure of the STATCOM.

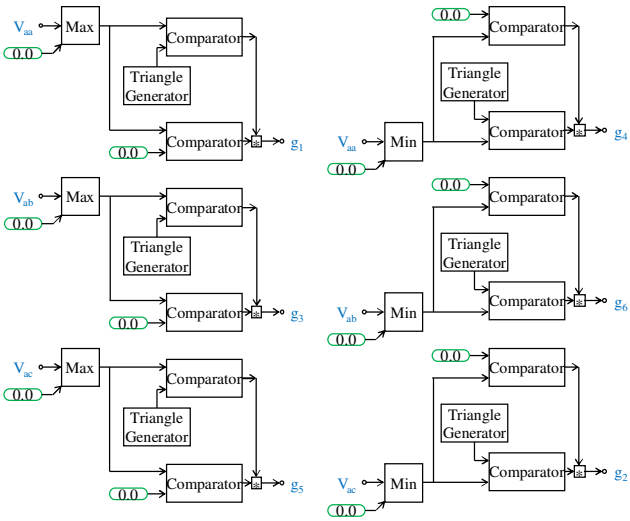

Fig. 8. Pulse generation block for STATCOM IGBTs.

V. SIMULATION RESULTS

The PSCAD program was utilized to simulate the proposed system. This system consists of an AC grid, a DC microgrid, and the STATCOM. The AC 3-phase system parameters are as follows: rated line voltage 11 kV, rated frequency 50 Hz, and Thevenin equivalent internal reactance 28.27 Ω. For current limiting purposes and adjusting the reactive and active power

transfer, a reactor with an inductance of 1.1 H is added between the PCC and the transformer. The DC microgrid has a voltage of 380 V. The microgrid system consists of a PV system with a maximum power of 60 kW, 4 wind models connected in parallel with a maximum power of 10 kW, 2 batteries with maximum power of 40 and 20 kW, and static loads with power of 80 kW. The transformation ratio of the transformer is set at 30 kV/380 V.

The STATCOM is operated to improve and keep the AC grid voltage at a constant value or near to the reference voltage and allow the transition of active power from and to the grid. In the event of a system disturbance causing a change in grid voltage, the STATCOM will be activated to restore and stabilize the voltage, bringing it back or close to the reference value. Three cases will be studied in which three loads will be added on the grid side after 5 s by using a circuit breaker. At first, the system operates in stable mode at 11 kV. Then, the load will enter the system and change the grid voltage. Finally, the STATCOM control will operate and enhance the system and bring back the grid voltage to 11 kV. The results will compare the grid voltage with the reference voltage. In two of the considered cases, the load causes a decrease in the grid voltage below 11 kV, while in the third case, the load leads to an increase in the grid voltage beyond 11 kV.

The first case, illustrated in Figure 9, involves the addition of an inductive load of 285 kVAR after the grid. Initially, the grid voltage starts at a steady state voltage of 11 kV. After 5 s, the grid voltage decreases to 10.3 kV. However, the control system eventually restores the voltage close to the reference value. Figure 10 depicts the second case where an inductive load of 135 kVAR is added to the grid at 5 s. Initially, the grid voltage starts at a steady state voltage of 11 kV. After 5 s, the grid voltage decreased to 10.65 kV. Subsequently, the control system restores the voltage back to the reference value. Figure 11 illustrates the third case where a capacitive load of 135 kVAR is added to the grid after 5 s. Similar to the previous case, the grid voltage begins at the steady state voltage of 11 kV. After 5 s, the grid voltage increases to 11.3 kV. Once again, the control system intervenes to bring the voltage back to the reference value.

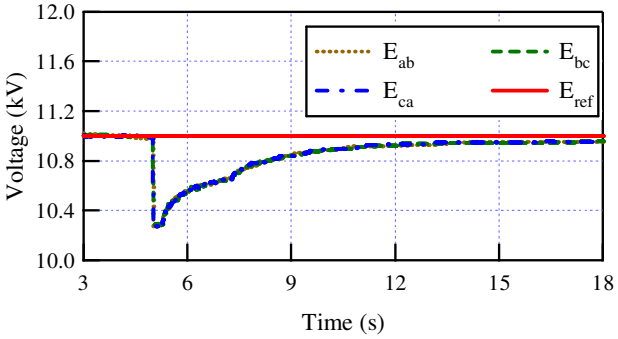

Fig. 9. Grid and reference voltage for inductive load of 285 kVAR.

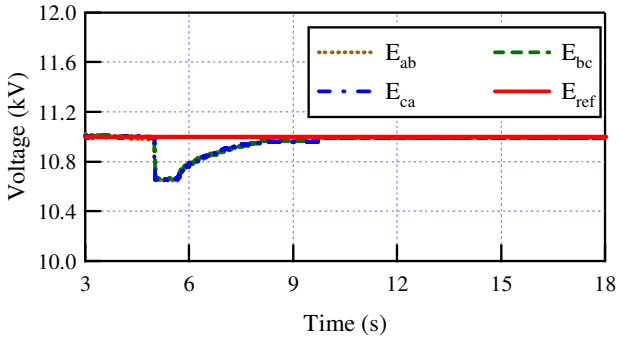

Fig. 10. Grid and reference voltage for inductive load of 135 kVAR.

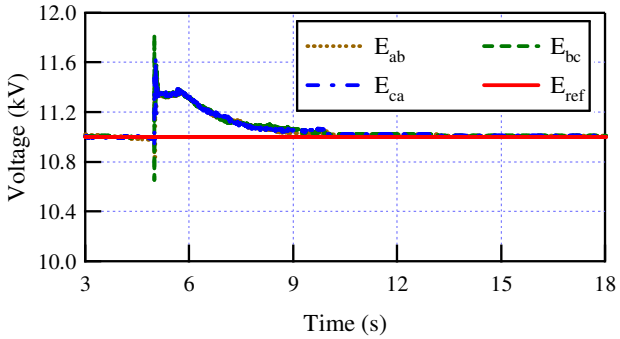

Fig. 11. Grid and reference voltage for capacitive load 135 kVAR.

In the first case, the grid voltage is improved but remains slightly below 11 kV due to the substantial difference between the grid voltage and the reference voltage. However, in the second and third cases, the grid voltage is successfully improved to 11 kV. The improvement in the voltage depends on reactive power. When the grid voltage reduces, the grid absorbs a certain amount of reactive power to compensate for the reduction of the voltage. When the grid voltage increases, the grid gives a certain amount of reactive power to compensate for that increase. The capacity of the microgrid determines its capability to provide reactive power support. Table I illustrates the value of reactive power compensation for the considered cases. It is evident that when the grid voltage is less than the reference voltage, the grid absorbs reactive power. This results in a negative value of reactive power, as illustrated in cases 1 and 2. Conversely, when the grid voltage surpasses the reference voltage, the grid supplies reactive power, leading to a positive value of reactive power, as seen in case 3. It is worth noting the discrepancy in the reactive power values between cases 1 and 2. In case 1, where there is a larger difference between the grid voltage and the reference voltage, the absorption of reactive power is greater than in case 2.

The system described here effectively facilitates the transfer of active power between the grid and the microgrid during both steady-state and transient conditions. The injection or absorption of 20 kW active power in the three cases is presented in Figures 12 and 13. Figure 12 displays the results of the microgrid's DC current for the three cases when active power is injected from the grid, resulting in a positive DC current. Figure 13 shows the DC current for the three cases

when the grid absorbs active power. In this scenario, the DC current of the microgrid becomes negative since the grid is drawing active power from the microgrid. Notably, the DC current value in case 1 is higher than that in case 2. This discrepancy is attributed to the varying load conditions in the two cases. When the load is larger, the DC current tends to be higher, and vice versa.

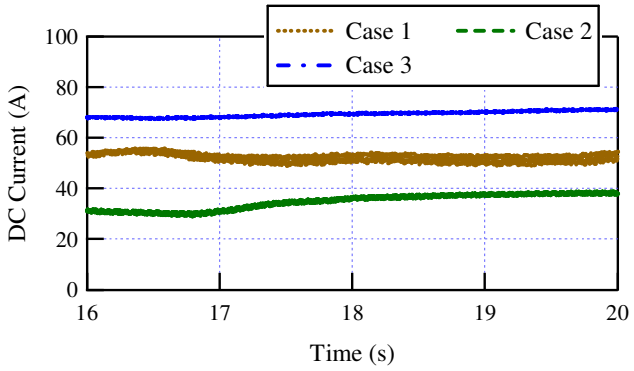

Fig. 12. The microgrid's DC current when active power is injected from the grid.

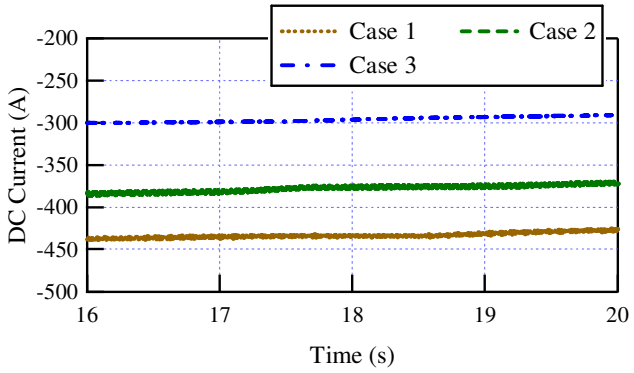

Fig. 13. The microgrid's DC current when the grid absorbs active power.

TABLE I. GRID VOLTAGE AND REACTIVE POWER

Cases	Load	Grid voltage	Reactive power
1	285 kVAR	10.3 kV	-60 kVAR
2	135 kVAR	10.65 kV	-50 kVAR
3	-135 kVAR	11.3 kV	45 kVAR

VI. REAL-TIME IMPLEMENTATION OF THE SYSTEM ON HIL PLATFORM

Typhoon HIL402 is a Hardware-In-the-Loop (HIL) real-time emulator that is frequently used for the design, testing, and test automation of power electronics control systems. Typhoon HIL platform is a valuable tool for validating the operation of the system. It contains a schematic editor that allows modeling and simulating the proposed system and controller. Typhoon HIL SCADA is a straightforward, user-friendly graphical environment that enables users to design custom interfaces with real-time models. The HIL SCADA program does two main tasks: it downloads simulation models to the HIL platform, and it manages the parameters, output, and emulation process. Many applications are performed on the HIL platform, such as the control development stage, automated converter controller testing, system integration stage, and interoperability testing.

Figure 14 shows the proposed system applied in the schematic editor of the HIL program. The system contains a 3-phase grid, a 3-phase transformer, a 3-phase converter, and a DC link. The objective of this system is to enhance the grid voltage and maintain it at its reference value. The 3-phase grid is star-earthed, and its specific details are provided in Table II. The 3-phase transformer is also star-earthed on both primary and secondary sides and has a transformation ratio of 40 kV/ 380 V. To manipulate the electrical signals by modifying, restructuring, or eliminating undesirable high frequencies, a 3-phase T-type low-pass filter is connected after the transformer, having L_2 = 0.009 mH, C_1 = 0.01 µF, and L_3 = 0.1 mH. The STATCOM, which consists of the 3-phase converter and the DC link, is also a part of the system. The 3-phase converter is controlled by a controller that regulates the voltage value, and it is equipped with 6 gates. The DC link is powered by a 380 V battery.

Figure 15 displays a visual representation of the testing setup for the proposed system, incorporating the HIL402 kit and a breakout board. To model the control circuits, the schematic editor within the Typhoon HIL control center is employed.

Figure 16 illustrates the control of the system. The Phase-Locked Loop (PLL) is used to obtain the value of wt and convert the 3-phase voltage into the dq frame. The PLL device has the same frequency as the system (50 Hz). The inputs to PLL are the instantaneous values of 3-phase voltage at PCC. The outputs of PLL are the voltages of the dq frame (V_d, V_q, and V_0) as shown in (5)-(7), the frequency (F), wt, and sin(wt). Frequency and sin(wt) are connected to termination because they were not used. In the HIL program, V_d represents the reactive power and V_q represents the active power. To improve the voltage, reactive power compensation is proposed. So, V_d is compared with the reference voltage and the error enters the PI controller as input and V_{d1} is obtained. Active power did not improve the voltage. So, V_q was compared to zero and the error entered the PI controller to obtain V_{q1}. The PI controller was adjusted at integral time constant (K_i) of 0.3 s and proportional gain (k_p) of 11. The outputs of the PI controller entered the dq0/abc device to convert the dq frame to abc frame as shown in (8)-(10). This device has a wt input with the same value as PLL. The waves from this device (V_{aa}, V_{ab}, and V_{ac}) are used to do PWM.

PWM is an effective technique used to divide an electrical signal into discrete portions, thereby reducing the average power delivered. This is achieved by rapidly switching the supply and load on and off, allowing for precise control over the average voltage and current delivered to the load. The simplest method for generating a PWM signal is the intersective approach, which involves using a triangle waveform (easily generated with a triangle generator) and a comparator device. Figure 17 illustrates this process, with the triangle generator producing a signal value of 8000 Hz.

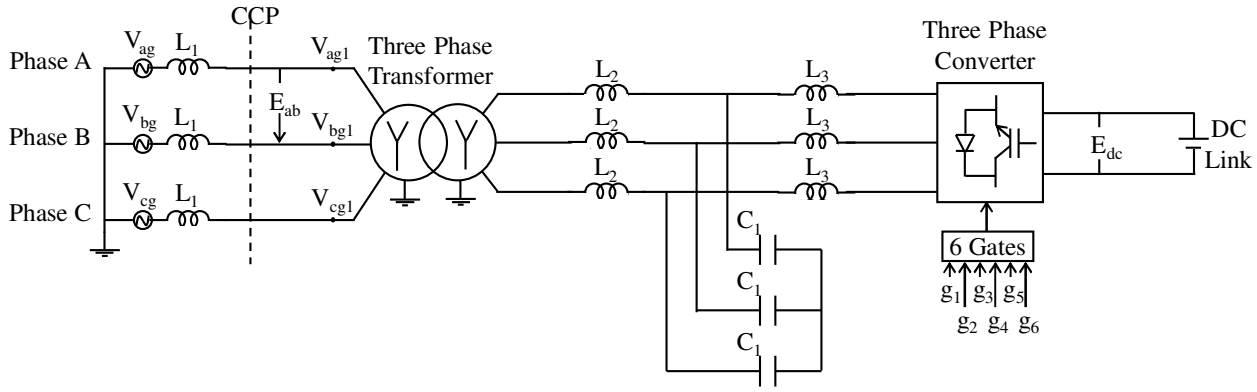

Fig. 14. The proposed system on Typhoon HIL 402.

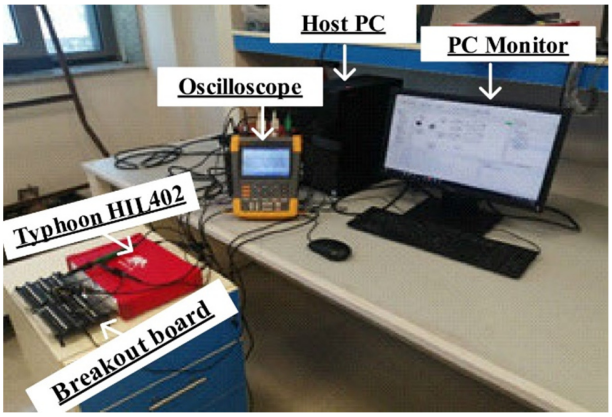

Fig. 15. Picture of the system implementation configuration based on Typhoon HIL 402.

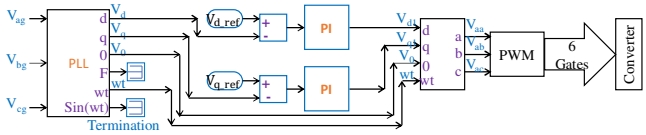

Fig. 16. Control structure of STATCOM.

TABLE II. GRID DETAILS

	Phase A	Phase B	Phase C
Line to line voltage	11 kV	11 kV	11 kV
Frequency	50 Hz	50 Hz	50 Hz
Phase angle	0 deg	-120 deg	120 deg
Internal inductance L_1	0.09 H	0.09 H	0.09 H

The system's results involve a comparison between the line voltage of the grid and the reference line voltage of 11 kV. These measurements were conducted under three different load conditions: an inductive load of 285 kVAR, an inductive load of 135 kVAR, and a capacitive load of 135 kVAR. The corresponding data are depicted in Figures 18-20. The results indicate that initially, the line voltage of the grid varies, but the control mechanism adjusts it to match the reference voltage.

The findings of this study highlight the significant advantages offered by the proposed system compared to previous research in the field. To provide a comprehensive overview and facilitate easy comparison, Table III summarizes the main features and characteristics of all relevant methods, including our system. This table highlights the strengths of the proposed system over the existing techniques.

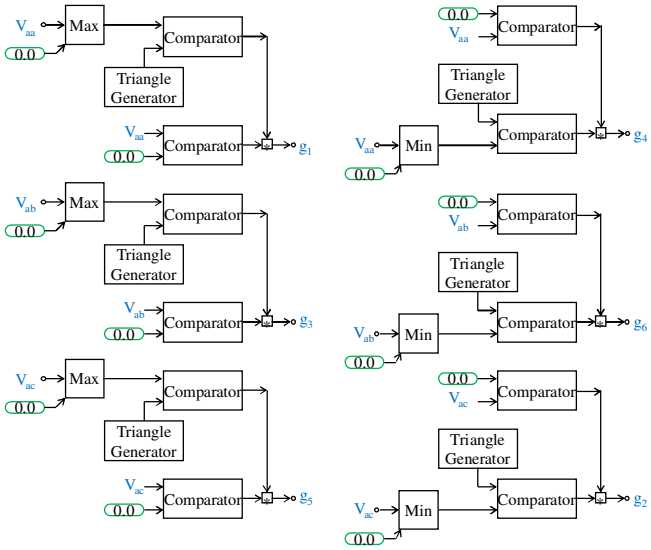

Fig. 17. PWM in Typhoon HIL device.

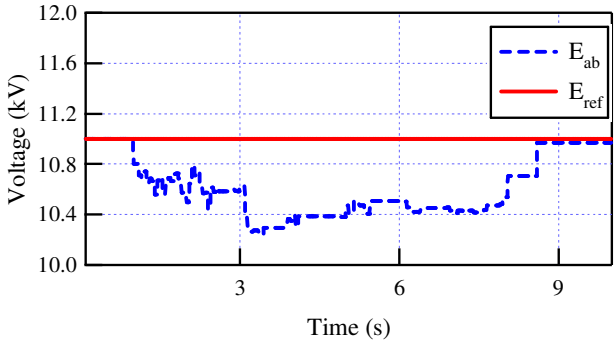

Fig. 18. Grid and reference voltage for inductive load of 285 kVAR.

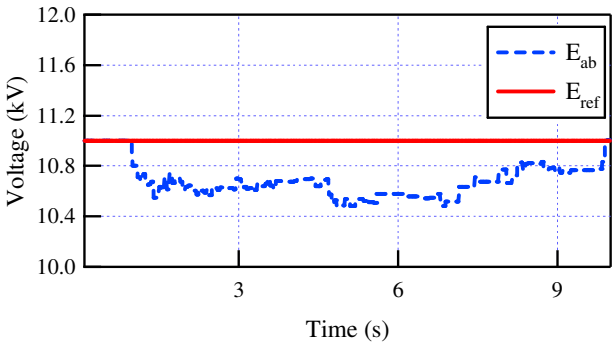

Fig. 19. Grid and reference voltage for inductive load of 135 kVAR.

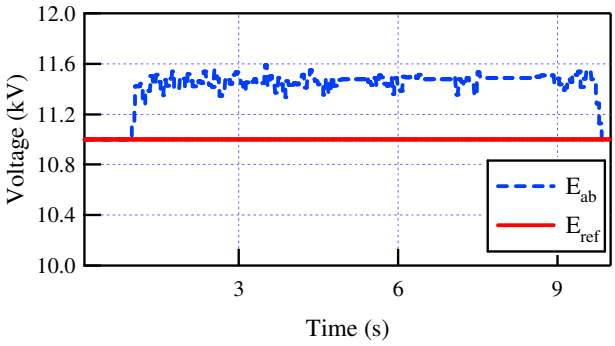

Fig. 20. Grid and reference voltage for capacitive load of 135 kVAR.

TABLE III. COMPARATIVE STUDY BETWEEN THE PROPOSED SYSTEM AND THE EXISTING LITERATURE

Ref.	Multiple energy sources	Reactive power control	Active power control	Control method / complexity	Real-time validation
[8]	X	√	√	PI controller / Meduim	X
[25]	√	√	√	Fuzzy-based / High	X
[26]	X	√	X	PI controller / Low	√
[27]	√	√	X	Neuro-Fuzzy / High	X
[28]	√	√	X	PI controller / Low	√
[29]	√	√	X	Genetic and Bacteria Foraging Algorithms / High	X
[30]	X	√	√	PI controller / Low	X
[31]	X	√	√	PI controller / Meduim	X
Proposed	√	√	√	PI controller / Low	√

VII. CONCLUSIONS

This paper proposes the use of STATCOM to connect an AC grid with a line voltage of 11 kV and a 380 V DC microgrid. The aim of this paper is to control the grid voltage at various conditions. To control the 3-phase system, at first the 3-phase system is converted to a dq system, then the control is applied on the dq system. STATCOM controls the reactive power compensation in order to control the grid voltage. The amount of injection of negative or positive reactive power depends on the difference between the grid voltage and the reference voltage. The system was simulated in the PSCAD package. The results of voltage are taken at three various cases of load at the common coupling point. In the first two cases, inductive load was added, decreasing the grid voltage below the reference voltage. In the third case, capacitive load was added, increasing the grid voltage higher than the reference voltage. The STATCOM control improved the grid voltage to its reference value. The proposed system also allows the transfer of the active power from and to the AC grid. The transition of active power is shown by studying the value of DC current at 0, 20, and -20 kW of active power transfer. At zero active power, the average DC current is approximately equal to zero. At the transition of 20 kW of active power, the average DC current is positive value. At -20 kW transition of active power, the average DC current is negative value. DC current is approximately equal to 500 A. At -50 kW transition of active power, the average DC current is approximately equal to -500 A. Finally, a real-time experiment was conducted and the results proved the effectiveness of the proposed control system.

REFERENCES

[1] P. A. Østergaard, N. Duic, Y. Noorollahi, and S. Kalogirou, "Renewable energy for sustainable development," *Renewable Energy*, vol. 199, pp. 1145–1152, Nov. 2022, https://doi.org/10.1016/j.renene.2022.09.065.

[2] F. Chien, C.-C. Hsu, I. Ozturk, A. Sharif, and M. Sadiq, "The role of renewable energy and urbanization towards greenhouse gas emission in top Asian countries: Evidence from advance panel estimations," *Renewable Energy*, vol. 186, pp. 207–216, Mar. 2022, https://doi.org/10.1016/j.renene.2021.12.118.

[3] G. Li, Y. Chen, A. Luo, and H. Wang, "An Enhancing Grid Stiffness Control Strategy of STATCOM/BESS for Damping Sub-Synchronous Resonance in Wind Farm Connected to Weak Grid," *IEEE Transactions on Industrial Informatics*, vol. 16, no. 9, pp. 5835–5845, Sep. 2020, https://doi.org/10.1109/TII.2019.2960863.

[4] A. Cagnano, E. De Tuglie, and P. Gibilisco, "Assessment and Control of Microgrid Impacts on Distribution Networks by Using Experimental Tests," *IEEE Transactions on Industry Applications*, vol. 55, no. 6, pp. 7157–7164, Nov.-Dec. 2019, https://doi.org/10.1109/TIA.2019.2940174.

[5] S. Pannala, N. Patari, A. K. Srivastava, and N. P. Padhy, "Effective Control and Management Scheme for Isolated and Grid Connected DC Microgrid," *IEEE Transactions on Industry Applications*, vol. 56, no. 6, pp. 6767–6780, Aug. 2020, https://doi.org/10.1109/TIA.2020.3015819.

[6] E. W. Nahas, H. A. Abd el-Ghany, D.-E. A. Mansour, and M. M. Eissa, "Extensive analysis of fault response and extracting fault features for DC microgrids," *Alexandria Engineering Journal*, vol. 60, no. 2, pp. 2405–2420, Apr. 2021, https://doi.org/10.1016/j.aej.2020.12.026.

[7] E. K. Belal, D. M. Yehia, and A. M. Azmy, "Effective Power Management of DC Microgrids Using Adaptive Droop Control," in *2018 Twentieth International Middle East Power Systems Conference (MEPCON)*, Cairo, Egypt, Sep. 2018, pp. 905–910, https://doi.org/10.1109/MEPCON.2018.8635164.

[8] R. K. Varma, E. M. Siavashi, S. Mohan, and T. Vanderheide, "First in Canada, Night and Day Field Demonstration of a New Photovoltaic Solar-Based Flexible AC Transmission System (FACTS) Device PV-STATCOM for Stabilizing Critical Induction Motor," *IEEE Access*, vol. 7, pp. 149479–149492, 2019, https://doi.org/10.1109/ACCESS.2019.2935161.

[9] R. K. Varma and H. Maleki, "PV Solar System Control as STATCOM (PV-STATCOM) for Power Oscillation Damping," *IEEE Transactions*

on Sustainable Energy, vol. 10, no. 4, pp. 1793–1803, Oct. 2019, https://doi.org/10.1109/TSTE.2018.2871074.

[10] P. Vaidya and V. K. Chandrakar, "Exploring the Enhanced Performance of a Static Synchronous Compensator with a Super-Capacitor in Power Networks," *Engineering, Technology & Applied Science Research*, vol. 12, no. 6, pp. 9703–9708, Dec. 2022, https://doi.org/10.48084/etasr.5317.

[11] Z. Liu, X. Hu, and Y. Liao, "Vehicle-Grid System Stability Analysis Based on Norm Criterion and Suppression of Low-Frequency Oscillation With MMC-STATCOM," *IEEE Transactions on Transportation Electrification*, vol. 4, no. 3, pp. 757–766, Sep. 2018, https://doi.org/10.1109/TTE.2018.2837623.

[12] L. Wang *et al.*, "Reduction of Three-Phase Voltage Unbalance Subject to Special Winding Connections of Two Single-Phase Distribution Transformers of a Microgrid System Using a Designed D-STATCOM Controller," *IEEE Transactions on Industry Applications*, vol. 54, no. 3, pp. 2002–2011, May-Jun. 2018, https://doi.org/10.1109/TIA.2017.2786707.

[13] A. Khoshooei, J. S. Moghani, I. Candela, and P. Rodriguez, "Control of D-STATCOM During Unbalanced Grid Faults Based on DC Voltage Oscillations and Peak Current Limitations," *IEEE Transactions on Industry Applications*, vol. 54, no. 2, pp. 1680–1690, Mar. 2018, https://doi.org/10.1109/TIA.2017.2785289.

[14] J. A. Suul, M. Molinas, and T. Undeland, "STATCOM-Based Indirect Torque Control of Induction Machines During Voltage Recovery After Grid Faults," *IEEE Transactions on Power Electronics*, vol. 25, no. 5, pp. 1240–1250, May 2010, https://doi.org/10.1109/TPEL.2009.2036619.

[15] J. Qi, W. Zhao, and X. Bian, "Comparative Study of SVC and STATCOM Reactive Power Compensation for Prosumer Microgrids With DFIG-Based Wind Farm Integration," *IEEE Access*, vol. 8, pp. 209878–209885, 2020, https://doi.org/10.1109/ACCESS.2020.3033058.

[16] R. Adware and V. Chandrakar, "Power Quality Enhancement in a Wind Farm Connected Grid with a Fuzzy-based STATCOM," *Engineering, Technology & Applied Science Research*, vol. 13, no. 1, pp. 10021–10026, Feb. 2023, https://doi.org/10.48084/etasr.5474.

[17] R. Adware and V. Chandrakar, "A Hybrid STATCOM Approach to Enhance the Grid Power Quality associated with a Wind Farm," *Engineering, Technology & Applied Science Research*, vol. 13, no. 4, pp. 11426–11431, Aug. 2023, https://doi.org/10.48084/etasr.6125.

[18] A. H. Elmetwaly, A. A. Eldesouky, and A. A. Sallam, "An Adaptive D-FACTS for Power Quality Enhancement in an Isolated Microgrid," *IEEE Access*, vol. 8, pp. 57923–57942, 2020, https://doi.org/10.1109/ACCESS.2020.2981444.

[19] E. Hashemzadeh, M. Aghamohammadi, M. Asadi, J. Z. Moghaddam, and J. M. Guerrero, "Secondary Control for a D-STATCOM DC-Link Voltage Under Capacitance Degradation," *IEEE Transactions on Power Electronics*, vol. 36, no. 11, pp. 13215–13224, Nov. 2021, https://doi.org/10.1109/TPEL.2021.3078182.

[20] E. W. Nahas, D.-E. A. Mansour, H. A. Abd el-Ghany, and M. M. Eissa, "Developing A Smart Power-Voltage Relay (SPV-Relay) with no Communication System for DC Microgrids," *Electric Power Systems Research*, vol. 187, Oct. 2020, Art. no. 106432, https://doi.org/10.1016/j.epsr.2020.106432.

[21] Y. Chen *et al.*, "Study on Electrothermal Characteristics of the Reverse-Conducting IGBT (RC-IGBT)," in *2020 21st International Conference on Electronic Packaging Technology (ICEPT)*, Guangzhou, China, Dec. 2020, pp. 1–5, https://doi.org/10.1109/ICEPT50128.2020.9202992.

[22] L. Xu, T. Chen, L. Yang, J. Chen, L. Du, and H. Zhong, "Reactive Power and Voltage Coordinated Control of Wind Farm for Parallel Running STATCOM," in *2019 IEEE Innovative Smart Grid Technologies - Asia (ISGT Asia)*, Chengdu, China, Feb. 2019, pp. 1414–1418, https://doi.org/10.1109/ISGT-Asia.2019.8880872.

[23] P. R. Kasari, M. Paul, B. Das, and A. Chakraborti, "Analysis of D-STATCOM for power quality enhancement in distribution network," in *TENCON 2017 - 2017 IEEE Region 10 Conference*, Penang, Malaysia, Aug. 2017, pp. 1421–1426, https://doi.org/10.1109/TENCON.2017.8228081.

[24] A. M. Amr, D.-E. A. Mansour, and A. E. ELGebaly, "Voltage Control of 11-kV AC Grid Using STATCOM Fed with DC Microgrid," in *2021 IEEE Conference of Russian Young Researchers in Electrical and Electronic Engineering (ElConRus)*, St. Petersburg, Moscow, Russia, Jan. 2021, pp. 1375–1381, https://doi.org/10.1109/ElConRus51938.2021.9396429.

[25] A. A. Nafeh, A. Heikal, R. A. El-Sehiemy, and W. A. A. Salem, "Intelligent fuzzy-based controllers for voltage stability enhancement of AC-DC micro-grid with D-STATCOM," *Alexandria Engineering Journal*, vol. 61, no. 3, pp. 2260–2293, Mar. 2022, https://doi.org/10.1016/j.aej.2021.07.012.

[26] S. Chakraborty, S. Mukhopadhyay, and S. K. Biswas, "Coordination of D-STATCOM & SVC for Dynamic VAR Compensation and Voltage Stabilization of an AC Grid Interconnected to a DC Microgrid," *IEEE Transactions on Industry Applications*, vol. 58, no. 1, pp. 634–644, Jan. 2022, https://doi.org/10.1109/TIA.2021.3123264.

[27] M. Lavanya and R. Shivakumar, "Performance Analysis of ANFIS-PSO based STATCOM in an Isolated Renewable Energy based Micro-Grid," *Journal of Scientific & Industrial Research*, vol. 81, no. 2, pp. 180–187, Feb. 2022, https://doi.org/10.56042/jsir.v81i02.37754.

[28] L. Ribeiro and D. Simonetti, "Voltage-Controlled and Current-Controlled Low Voltage STATCOM: A Comparison," in *20th International Conference on Renewable Energies and Power Quality (ICREPQ'22)*, Vigo, Spain, Sep. 2022, vol. 20, pp. 536–541, https://doi.org/10.24084/repqj20.358.

[29] H. Bakir and A. A. Kulaksiz, "Modelling and voltage control of the solar-wind hybrid micro-grid with optimized STATCOM using GA and BFA," *Engineering Science and Technology, an International Journal*, vol. 23, no. 3, pp. 576–584, Jun. 2020, https://doi.org/10.1016/j.jestch.2019.07.009.

[30] P. O. Dorile, D. R. Jagessar, L. Guardado, S. S. Jagessar, and R. A. McCann, "Power System Stabilization of a Grid Highly Penetrated from a Variable-Speed Wind Based Farm Through Robust Means of STATCOM and SSSC," in *2021 16th International Conference on Engineering of Modern Electric Systems (EMES)*, Oradea, Romania, Jun. 2021, pp. 1–6, https://doi.org/10.1109/EMES52337.2021.9484110.

[31] A. B. Chivukula and S. Maiti, "Analysis and control of modular multilevel converter-based E-STATCOM to integrate large wind farms with the grid," *IET Generation, Transmission & Distribution*, vol. 13, no. 20, pp. 4604–4616, Oct. 2019, https://doi.org/10.1049/iet-gtd.2018.5928.